Removal of phosphate from solution using lanthanum-modified wheat straw

Yuanyuan Wang[a,b], Xu Liu[b], Yuwei Song[b], Runping Han[b,*]

aCollege of Ecology and Environment, Zhengzhou University, email: 2305942027@qq.com (Y.Y. Wang)
*bCollege of Chemistry, Zhengzhou University, No. 100 of Ke xue Road, Zhengzhou, 450001, China, emails: lxcod@zzu.edu.cn (X. Liu),
1542682693@qq.com (Y.W. Song), rphan67@zzu.edu.cn (R.P. Han)*

ABSTRACT

It is valuable to remove phosphate from solution and adsorption is often considered. In this study, wheat straw (WS) was modified with lanthanum hydroxide to investigate the adsorption property of materials towards phosphate from solution. The WS and modified WS (La-WS) were characterized by Fourier-transform infrared spectroscopy, scanning electron microscopy, X-ray fluorescence analysis, which showed that La was loaded on the surface of WS. The pH range for PO_4^{3-} adsorption onto La-WS was wide and the effect of salinity was not significant. The adsorption capacity of WS was significantly improved after modification and the adsorption capacity from experiments was to 34.5 mg·g^{-1} at 303 K. The Langmuir model could well describe the equilibrium results and the process was dominated by the adsorption of single molecular layer. The pseudo-second-order kinetic model could better describe the kinetics process and the process was mainly chemisorption. The column adsorption studies showed that the lower the flow rate, the higher the column height and initial PO_4^{3-} concentration were in favor of adsorption capacity. The process was spontaneous and endothermic from thermodynamic analysis. The Thomas model could better describe the process of PO_4^{3-} adsorption onto La-WS and 0.1 mol·L^{-1} NaOH solution had better regeneration effect of PO_4^{3-}-loaded La-WS. As environmentally friendly and economic materials, La-WS is promising to remove phosphate from real wastewater.

Keywords: Modified wheat straw; Phosphate; Adsorption; Regeneration

1. Introduction

Phosphorus is an essential element necessary for biological growth and development. However, the overuse of phosphorus-containing pesticides and fertilizers in agriculture has led to excessive phosphorus discharge into water bodies [1], resulting in eutrophication [2,3], which threatens the water environment and human health. So it is essential to remove phosphate from solution. The main methods of phosphorus removal from wastewater include electrolysis [4], chemical precipitation [5], crystallization [6], adsorption [7], biofilm [8], etc.

Currently, various composite materials are widely used for phosphorus removal by adsorption [9]. For example,

organometallic skeletons [10], layered double hydroxides [11], minerals [12], and biomass [13] are used to remove phosphate from wastewater. However, many composite materials are economically costly and prone to secondary pollution. Therefore, it is necessary to find composite materials with low cost, high adsorption efficiency and easy recovery.

As one of a large yielding and renewable biomass, wheat straw (WS) is widely used in paper, board, livestock feed, biofuel and other fields [14]. WS is rich in lignin and has a large specific surface area [15], which is increasingly used as an adsorbent to bind pollutants from water. However, due to its some negative functional groups and low surface [16], it has poor adsorption capacity of pollutants in general, especial for anionic pollutants [17]. Therefore,

* Corresponding author.

physicochemical methods are usually used to modify the WS to improve the adsorption performance of wheat straw. These include ultrasonic method [18], high temperature charring method [19], acid-base modification method [20], surfactant modification method [21], amine modification method [22], etc. Mood et al. [23] combined WS with pyrolytic activation into nitrogen-magnesium co-doped (NMD) coke to adsorb phosphate in aqueous solution, and the phosphate adsorption capacity could reach 122 mg·g⁻¹. Tang et al. [24] modified WS with palmitic acid to reduce the density of hydroxyl groups existed in wheat straw through esterification reaction and improve the oil adsorption rate and the performance of oil spill clean-up were improved by esterification, thus producing a low-cost, degradable and efficient oil adsorbent. The modified wheat straw could absorb oil up to 24.3 mg·g⁻¹. Ma et al. [25] conducted a series of batch experiments by graft copolymerization with wheat straw, acrylic acid (AA), acrylic acid (AM) and methyl diallyl ammonium chloride (DMDAAC) to investigate the effects of solution pH, adsorbent dosage, concentration of adsorbate and contact time. The results showed that the new fertilizer control agent had a significant effect on the adsorption of ammonium and phosphate ions [25].

Lanthanum-modified materials have high affinity for phosphate and can form complexes between lanthanum and phosphate even at low concentrations [26–28]. Therefore, lanthanum-modified materials are widely used for removal of phosphate [29]. Zhang et al. [30] modified various crop straws with lanthanum hydroxide to remove phosphorus from livestock and poultry farming wastewater. The maximum adsorption capacity of modified ginger stalk was 52 mg·g⁻¹. Huang et al. [31] found that amine-modified wheat straw biochar, lanthanum-modified wheat straw biochar had a shorter adsorption time to reach equilibrium and high phosphorus removal efficiency, with an adsorption capacity of 172 mg·g⁻¹ and 99.98% phosphorus removal. And it still had good adsorption performance at low phosphate concentration.

In this study, WS was used as a sustainable support material and lanthanum hydroxide was used to modify WS to prepare an economical and sustainable adsorbent, and its phosphorus adsorption performance was investigated under different conditions through batch and column adsorption.

2. Materials and methods

2.1. Materials and instruments

Wheat straw (WS) was obtained from local countryside and WS (40–60 mesh) was selected after pretreatment. Reagents: $LaCl_3 \cdot 7H_2O$, NaCl, Na_2SO_4, HCl, NaOH, KH_2PO_4, KNO_3. The test reagents were all analytically pure, and the water used in the experiment was distilled water.

The pH at point of zero charge (pH_{zpc}) of WS and La-WS were measured by the solid addition method using the PHS-3C meter (INESA, PHS-3C, China). The chemical groups of WS, NWS, La-WS were analyzed by Fourier-transform infrared spectroscopy (FTIR, PE-1710FTIR, USA). The X-ray fluorescence analysis was used to determine the content of each element in wheat straw before and after modification

(XRF, S4 PIONEER, Germany). The morphology and microstructure of La-WS was observed by scanning electron microscopy (SEM, Zeiss/Auriga, Holland).

2.2. Pretreatment of wheat straw

The wheat straw (2.0 g) was reacted with 100 mL NaOH (1 mol·L⁻¹) at 30°C for 2 h. The liquid pH was increased to 10.0 and the temperature of the above mixture was raised to 60°C, washed with distilled water to neutral and then filtered and dried in a vacuum oven at 80°C and set aside, labeled as WS.

2.3. Pretreatment of La-WS

WS (2.0 g) was added to 100 mL of lanthanum chloride (50 mg·L⁻¹) solution and shaken at 30°C for 30 min, then the pH of the solution was adjusted to 10.0 with NaOH (2 mol·L⁻¹), and then shaken at 50°C for 16 h. The solid was filtered and washed with distilled water until no white precipitation appeared by $AgNO_3$ test, dried in a vacuum oven at 80°C and set aside to obtain lanthanum-loaded wheat straw, labeled as La-WS.

2.4. Batch adsorption experiments

A certain amount of La-WS was sealed in 50 mL flask by adding 10 mL of a certain concentration of phosphate solution, and then shaken at a constant temperature of 303 K for 6 h. The effects of solution pH (1~11), adsorbent concentration (0.1~2.0 g·L⁻¹), salinity (0~0.12 mol·L⁻¹ NaCl and Na_2SO_4) and adsorption temperature (303, 313, and 318 K) were investigated. The pH of the phosphate solution was adjusted with NaOH and HCl solutions and also monitored with a pH meter. The concentration of phosphate after adsorption was measured by obtaining the absorbance at 700 nm using molybdenum antimony spectrophotometry (Ultraviolet-Visible Spectrophotometer, UV, 752, China). The calculation of unit adsorption and removal efficiency is obtained from Eqs. (1) and (2).

$$q = \frac{(C_0 - C)V}{m} \tag{1}$$

$$p = \frac{(C_0 - C)}{C_0} \tag{2}$$

where q (mg·L⁻¹) is the unit adsorption amount, m (g) is the mass of adsorbent, V (L) is the volume of adsorbent solution, C_0 (mg·L⁻¹) is the concentration of adsorbent before adsorption, C (mg·L⁻¹) is the concentration of PO_4^{3-} at time t or equilibrium, and p (%) is the removal efficiency.

The tests were performed in triplicate and the average was recorded for accuracy and reproducibility.

2.5. Column adsorption experiments

A certain amount of La-WS (such as 0.576 g, 4.7 cm) was filled in the column (length 30 cm, inner diameter 1 cm) as fixed bed. A certain concentration of PO_4^{3-} solution (pH near 7.0) was pumped into the column by a mobile pump from top to bottom, and the effluent was picked up at

regular intervals and the concentration of PO_4^{3-} was measured. Various parameters, such as bed height, flow rate and solution concentration, were performed. The breakthrough curves ($C_t/C_0 \sim t$) can be performed. The total adsorption amount Q_m (mg) of pollutants by the modified wheat straw adsorption column can be calculated by integration from Eq. (3), and t_{total} (min) is the total time of the whole dynamic adsorption reaction.

$$Q_m = \frac{v}{1,000} \sum_{t=0}^{t=t_{total}} (C_0 - C_t) dt \qquad (3)$$

The unit adsorption capacity of MWS for anionic pollutants can be expressed by Eq. (4):

$$q_e = \frac{Q_m}{m} \qquad (4)$$

The total mass of adsorbent W_{total} (mg) flowing into the adsorption column during the whole adsorption time total during dynamic adsorption can be obtained from Eq. (5):

$$W_{total} = \frac{vC_0 t_{total}}{1000} \qquad (5)$$

The removal efficiency Y (%) of pollutants by MWS can be calculated by Eq. (6):

$$Y = \frac{Q_m}{W_{total}} \times 100\% \qquad (6)$$

where v (mL·min⁻¹) is the flow rate, t (min) is the dynamic adsorption time, C_0 (mg·L⁻¹) is the concentration of influent, C_t (mg·L⁻¹) is the concentration of the effluent at time t, Q_m (mg) is the total amount of adsorbed pollutant, and t_{total} (min) is the total dynamic adsorption reaction time.

2.6. Desorption tests

Since the lanthanide-modified adsorbent material had good regeneration ability in NaOH solution [31], 0.01 mol·L⁻¹ NaOH solution was selected for desorption studies. Specifically, 0.05 g of La-WS was added to flask with 10 mL 50 mg·L⁻¹ phosphate solution, and shaken at a constant temperature of 303 K for 6 h until complete adsorption saturation. The samples were filtered and washed, then spent material was transferred to 0.01 mol·L⁻¹ NaOH solution, maintaining a solid–liquid ratio of 1:1 (m/V). The samples were then shaken for 48 h and filtered with water until the pH value was neutral. The obtained samples were dried at 60°C under vacuum and used. The above procedure was repeated three times.

Similarly, spent adsorbent after column adsorption was also regenerated and reused.

3. Results and discussion

3.1. Characterization of materials

3.1.1. Determination of isoelectric point

To understand the electrical properties of WS and La-WS surface, the study was conducted to determine the isoelectric point [32]. As shown in Fig. 1, with the increase

of pH, values of ΔpH first increased and then decreased. When the charge was zero, the isoelectric point of WS was 7.67 and that of La-WS was 7.44. The isoelectric point of La-WS decreased slightly relative to the WS isoelectric point. The surface charge of WS moved in the acidic direction, indicating that lanthanum was loaded onto WS. La-WS had the highest positive charge content at pH = 3, indicating that phosphate adsorption may be best at pH = 3 [33].

3.1.2. FTIR analysis

In order to compare the differences of surface functional groups before and after the modification of wheat straw [34], WS and La-WS were analyzed by FTIR to confirm the functional groups on the surface, and the results were shown in Fig. 2. It was clearly seen from Fig. 2a that the peak of C=O from the conjugated carbonyl group was located at 1,734 cm⁻¹. The phenolic hydroxyl absorption peak was located at 1,300 cm⁻¹. The absorption at 1,265 cm⁻¹ was due to the cyclic methoxy stretching vibration. The C–O–C absorption peak in the characterized ester bond was at 1,147 cm⁻¹ while the C–O absorption peak was at 1,051 cm⁻¹. The characteristic absorption peak of different substitution types of benzene ring was enhanced at 665 cm⁻¹. From Fig. 2b, it could be seen that the absorption peaks of –OH were significantly enhanced near 3,400 cm⁻¹ and there was a significant increase in hydroxide precipitated polymer, which indicated enhanced hydrogen bonding and thus a stronger adsorption capacity of La-WS [35]. But the peaks from vibration of C=O, C–O–C disappeared or weakened. This indicated that the lignin structure of WS was partially destroyed after pretreatment with sodium hydroxide, and some functional groups such as –OH, –CH₂, –OCH₃, C–O–C were broken, while the substitutable aromatic structures were increased. Several distinct new peaks in Fig. 2b are present from 500 to 670 cm⁻¹, which represent the vibrational peaks of La-OH bond, indicating that La was successfully loaded on wheat straw.

3.1.3. XRF analysis

As shown in Table 1, the content of each element in wheat straw before and after modification was determined
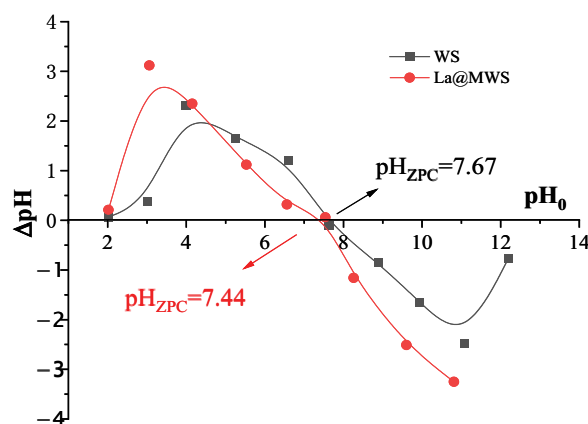

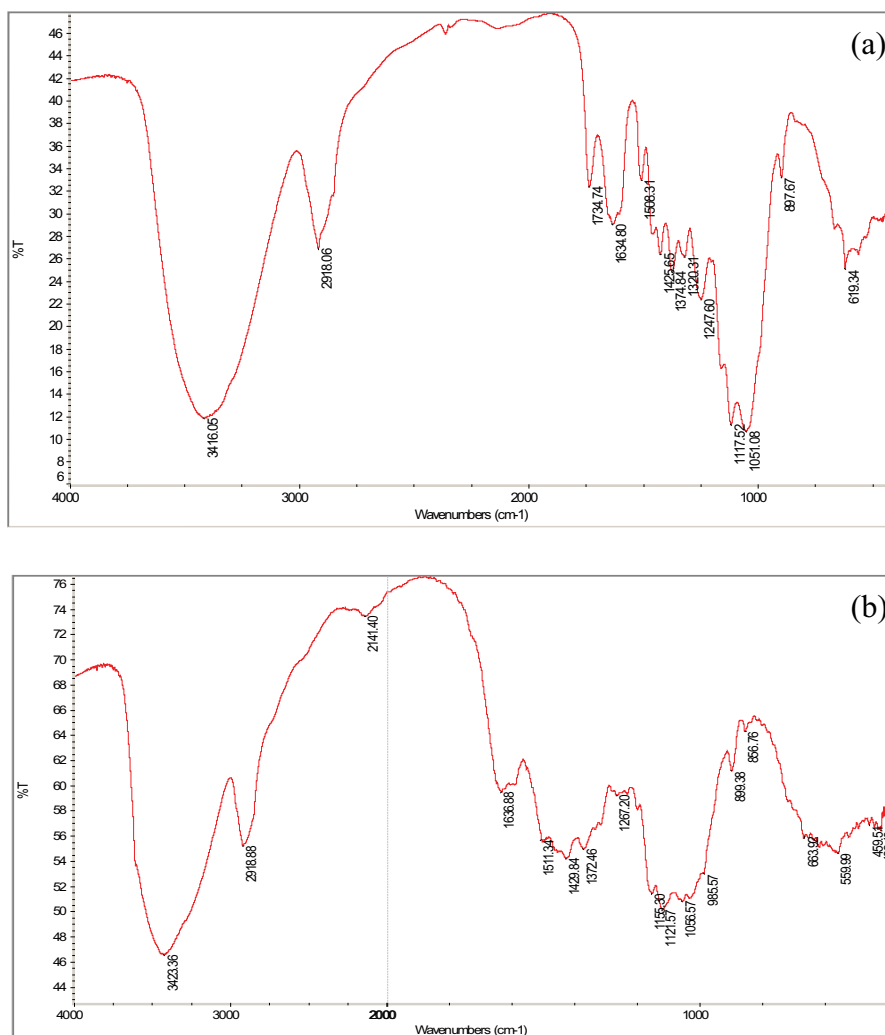Fig. 1. Isoelectric point diagram of wheat straw before and after modification.

Fig. 2. Infrared spectra of wheat straw before and after modification (a) WS and (b) La-WS).

Table 1
X-ray fluorescence analysis of WS and La-WS

Formula	Z	WS (%)	La-WS (%)
O	8	2.920	9.210
Mg	12	0.063	0.081
Si	14	1.891	0.783
S	16	0.171	0.063
Cl	17	0.264	0.534
Ca	20	1.220	0.752
La	57	–	46.28
Fe	26	0.079	–

semi-quantitatively by XRF analysis [36]. For NW, there is not detection of La while there is 46.3% La about La-WS. The content of La increased obviously, indicating that lanthanum was successfully loaded on WS mostly in the form of lanthanum hydroxide (according to condition of preparation).

3.1.4. SEM analysis

To understand the morphological changes of wheat straw before and after modification, SEM was used for analysis, and the results are shown in Fig. 3. The surface of WS was relatively rough and showed a hollow shape inside (Fig. 3a). After La modification, there was more pore on the surface (Fig. 3b), which indicated that lanthanum had been successfully loaded on the wheat straw and also explained the increased adsorption capacity of La-WS toward phosphate from solution.

3.2. Batch adsorption studies

3.2.1. Effect of adsorbent dosage

The effect of La-WS dosage on phosphate adsorption was studied in order to improve the utilization of adsorbent, reduce the cost and avoid wasting resources. As could be seen in Fig. 4a, with increasing concentration of La-WS, the removal efficiency (p) of PO_4^{3-} first increased rapidly and then tended to equilibrate, while the unit adsorption
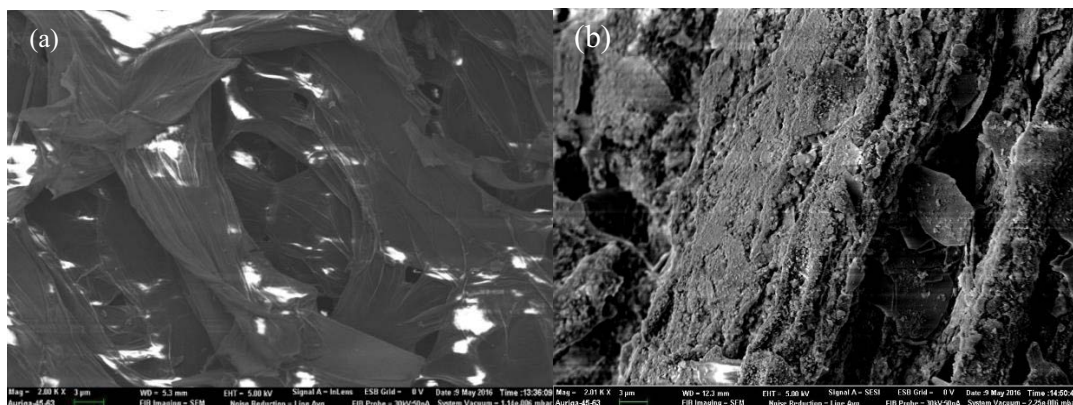
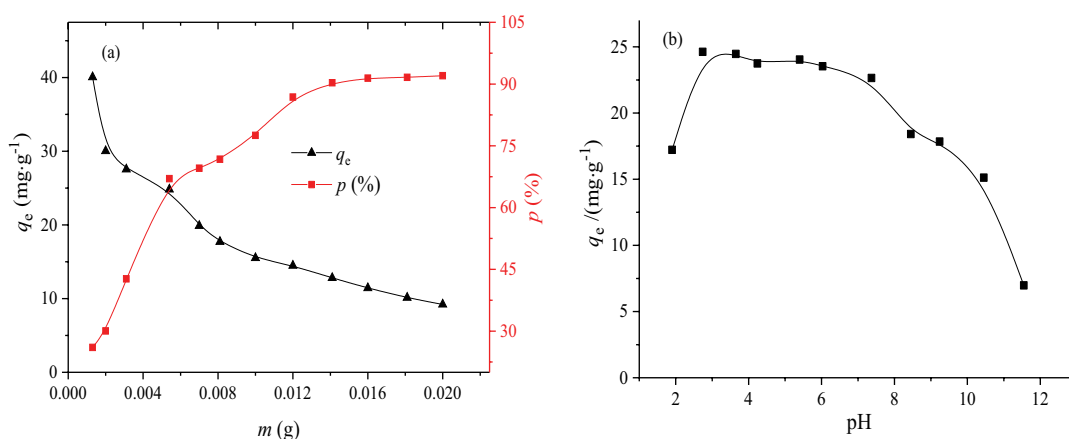Fig. 3. Scanning electron micrographs before and after modification (a) WS and (b) La-WS).

Fig. 4. Effect of dose (a) and solution pH (b) on adsorption.

amount q_e of PO_4^{3-} became lower and lower. This was due to a decrease in the amount of relatively bound adsorbates as the dose increased, which led to a decrease in the unit adsorption capacity. When the adsorbent concentration was 0.5 g·L⁻¹, the removal rate of PO_4^{3-} from the solution was 67.0% and the unit adsorption amount was 24.9 mg·g⁻¹. To ensure the utilization of La-WS, the adsorbent concentration of 0.5 g·L⁻¹ was chosen for the experiment. At same conditions, the value of q_e about WS is 4.52 mg·g⁻¹. This confirmed the value of La modification.

3.2.2. Effect of pH

The solution pH can affect the form of adsorbate and property of adsorbent surface, then affect adsorption quantity. The adsorption of phosphate at pH values in the range of 2–12 was studied as shown in Fig. 4b.

When the solution pH was less than 3 or greater than 7, the unit adsorption capacity decreased rapidly. When the pH was less than 3, the solution existed mainly in the form of phosphate acid, which was not easily absorbed by La-WS. When the solution pH was greater than 7, as the acidity decreased, phosphate formed competition with OH⁻ for adsorption [37]. When the solution pH was between 3 and 7, the phosphate in solution existed mainly in the form of

dihydrogen salts (H_3PO_4: pK_{a1} = 2.16, pK_{a2} = 7.20, pK_{a3} = 10.3), which was easily adsorbed by La-WS [38]. In summary, La-WS had a high adsorption capacity for PO_4^{3-} over a wide range of solution pH, and the pH of phosphorus-enriched wastewater was generally around 7. Considering the practical application, no further adjustment of the solution pH (near 7.0) was required in the subsequent study.

3.2.3. Effect of salinity

For investigating the effect of salinity, this experiment explored the effect of two salts (NaCl and Na_2SO_4). The study found (figure not shown) that Cl⁻ and SO_4^{2-} had little effect on the removal of PO_4^{3-} from water by La-WS, with unit adsorption amounts fluctuating around 25 mg·g⁻¹. This indicated that La-WS was capable of selective adsorption of phosphate [39]. Another researcher used similar metal oxides for PO_4^{3-} adsorption studies and obtained the same results, which were mainly due to the formation of complexes in the inner layer [40].

3.2.4. Study of adsorption equilibrium

As shown in Fig. 5a, as the temperature increased, the values of q_e about phosphate onto La-WS increased,
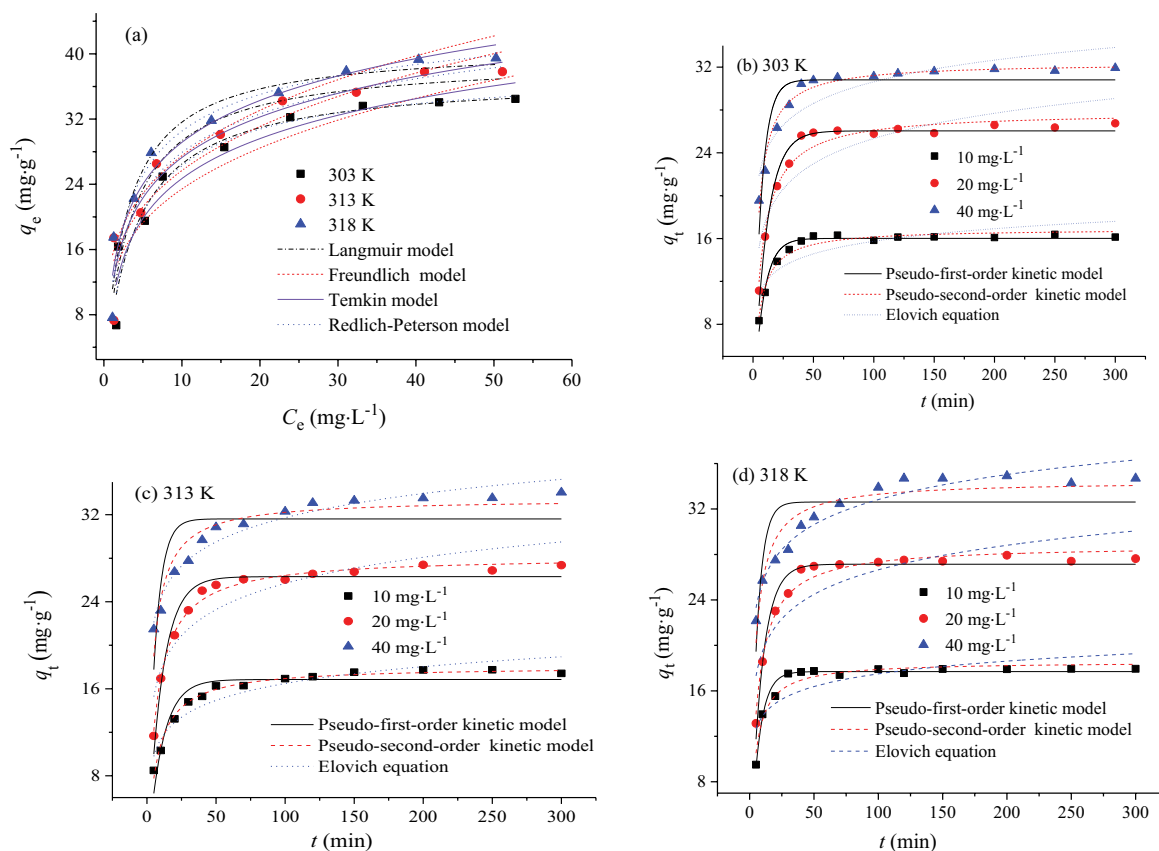
Fig. 5. Kinetic curves of PO_4^{3-} adsorption onto La-WS (a) 303 K, (b) 313 K, (c) 318 K; adsorption isotherm curves at various temperatures (d).

indicating that this adsorption process was endothermic. At a certain temperature, the unit adsorption amount q_e increased rapidly at low concentrations, which was due to the fact that the adsorption saturation had not reached saturation in the low concentration range. As the phosphate concentration increased, the adsorption gradually reached saturation and q_e increased slowly until equilibrium. The experimental adsorption amounts of La-WS toward phosphate were 34.5 and 39.5 mg·g⁻¹ at 303 and 318 K, respectively.

To further explore the adsorption mechanism and investigate the effect of temperature on the adsorption of La-WS on phosphate, the adsorption process was fitted non-linearly by four isothermal models, and the expressions of models were shown in Table 2.

The determination of the degree of conformity of each adsorption model to the adsorption isotherm was based mainly on the principle of least squares and determined coefficient (R^2). If the values of R^2 are closer to 1 and the error value was smaller, relative model is suitable to fit the process. The fitted results using non-linear regressive analysis are shown in Table 3 and the fitted curves are also presented in Fig. 5a.

Compared to Freundlich model, there are higher values of R^2 and smaller values of SSE, while values of q_m from this model were closer to the values from experiments. Furthermore, the fitted curves from Langmuir model were

also closer to experimental curves, indicating that Langmuir model can describe the equilibrium adsorption process and max adsorption quantity and the process was dominated by the uniform adsorption of a single molecular layer [41].

The Temkin model was commonly used to describe multiphase surface adsorption. As the R^2 value was lower and the SSE value was higher, and the fitted parameters were less suitable for describing this adsorption process.

The Redlich–Peterson adsorption model was a combination of the Freundlich and Langmuir models [42]. The g values fitted by this model were 0.977, 0.882 and 0.924, which were closer to 1, so the model was more inclined to the Langmuir model. Langmuir model had the highest fit among the models analyzed, so Langmuir was able to describe the adsorption behavior well, indicating that the adsorption process was mainly dominated by monolayer homogeneous adsorption and supplemented by multilayer non-homogeneous adsorption.

3.2.5. Adsorption kinetics study

The kinetic curves at various conditions are shown in Fig. 5b–d. It could be seen that the unit adsorption amount increased rapidly with increasing time at constant temperature, and then the increase became slow until equilibrium was reached, indicating that the adsorption process was a fast one [43]. From Fig. 5b, the time to reach equilibrium

Table 2
Adsorption models applied in this study

Adsorption models	Expression	Parameters
		Isotherm models
Langmuir model	$q_e = \dfrac{q_m K_L C_e}{1 + K_L C_e}$	q_e is the equilibrium adsorption quantity (mg·g^{-1}), C_e is the AR concentration at equilibrium (mg·L^{-1}), K_L is the Langmuir binding constant related to the free energy of adsorption (L·mg^{-1}), q_m is the maximum adsorption capacity (mg·g^{-1})
Freundlich model	$q_e = K_F C_e^{1/n}$	K_F and $1/n$ are the Freundlich constants characteristics of the system, implying the adsorption capacity and the adsorption intensity
Redlich–Peterson model	$q_e = \dfrac{A C_e}{1 + B C_e^g}$	A, B and g are the Redlich–Peterson parameters, g means the degree of heterogeneity, between 0 and 1. If the value of g is 1, the equation is equal to Langmuir
Temkin model	$q_e = A + B \ln C_e$	A and B are parameters of Temkin model
		Kinetic models
Pseudo-first-order kinetic equation	$q_t = q_e \left(1 + e^{-k_1 t} \right)$	q_e is the equilibrium adsorption quantity (mg·g^{-1}) and k_1 is the rate constant of the equation (min^{-1})
Pseudo-second-order kinetic equation	$q_t = \dfrac{k_2 q_e^2 t}{1 + K_2 q_e t}$	k_2 is the rate constant of the equation (g·mg^{-1}·min^{-1})
Elovich equation	$q_t = \dfrac{\ln(\alpha\beta)}{\beta} + \dfrac{\ln t}{\beta}$	α is the initial adsorption rate constant (mg·g^{-1}·min^{-1}); β is related to the extent of surface coverage and activation energy for chemisorption (g·mg^{-1})
		Column models
Thomas model	$\dfrac{C_t}{C_0} = \dfrac{1}{1 + \exp\left(K_{Th} q_0 m / v - k_{Th} C_0 t \right)}$	C_0 and C_t denote the inlet and outlet concentration (mg·L^{-1}), respectively; K_{Th} is constant for the Thomas model (mL·min^{-1}·mg^{-1}), q_0 represents the maximum amount adsorbed (mg·g^{-1}), m is the mass of La-WS (g), and v is the feed rate (mL·min^{-1})
Clark model	$\dfrac{C_t}{C_0} = \left(\dfrac{1}{1 + A e^{-rt}} \right)^{1(n-1)}$	A and r is the Clark's constant while n is from Freundlich model

was about 50 min for a solution with an initial concentration of 10 mg·L^{-1}, while the solution with an initial concentration of 40 mg·L^{-1} still did not reach equilibrium at 50 min and reached equilibrium at 120 min, which also indicated that highly concentrated solutions tend to take longer to reach equilibrium. At the temperature of 318 K, the values of adsorption quantity were 17.9, 27.9, and 34.7 mg·g^{-1} with initial the concentrations 10, 20 and 40 mg·L^{-1}, respectively. This also indicated that the unit adsorption amounts increased with the increase of the solution concentrations.

To describe the adsorption efficiency of the adsorbent, three common kinetic models were used to fit the non-linear process of phosphate adsorption by La-WS. The expressions of kinetic models are also shown in Table 2.

The fitted results are shown in Table 4 and Fig. 5b–d. It was seen from Table 4 that the pseudo-second-order kinetic model had the smallest error value, the largest R^2 and a smaller gap between the theoretical adsorption $q_{e(theo)}$ and experimental adsorption $q_{e(exp)}$. The fitted curves from this model were closer to experimental points. So, the pseudo-second-order kinetic model could well describe the adsorption process. The Elovich model was used to describe

the heterogeneous diffusion process. From the fitted data, it was clear that there was no specific trend in the variation of parameters α and β in the Elovich model as the initial concentration of phosphate solution increases. The determined coefficient R^2 was low and the error was large, so the Elovich model was not suitable to describe the adsorption process. In general, the adsorption process of phosphate was mainly chemisorption.

3.2.6. Adsorption thermodynamics study

To study the effect of temperature adsorption and to reveal its thermodynamic properties, the thermodynamic parameters are calculated by the following expressions:

$$\ln K_L = \frac{\Delta S^\circ}{R} - \frac{\Delta H^\circ}{RT} \tag{7}$$

$$\Delta G^\circ = \Delta H^\circ - T \Delta S^\circ \tag{8}$$

$$\ln k = -\frac{E_a}{RT} + \ln A \tag{9}$$

Table 3
Fitting results of isotherm models toward PO_4^{3-} adsorption on La-WS

		Langmuir			
T (K)	K_L (L·mg^{-1})	$q_{m(exp)}$ (mg·g^{-1})	$q_{m(theo)}$ (mg·g^{-1})	R^2	SSE
303	0.247	34.5	37.2	0.937	41.1
313	0.291	37.8	39.4	0.911	68.9
318	0.338	39.5	41.0	0.944	47.8
		Freundlich			
T (K)	$q_{m(exp)}$ (mg·g^{-1})	K_F	$1/n$	R^2	SSE
303	34.5	12.3	0.281	0.867	87.0
313	37.8	13.6	0.276	0.890	85.1
318	39.5	14.9	0.266	0.895	90.0
		Temkin			
T (K)	A	B	R^2		SSE
303	8.43	7.07	0.922		51.1
313	10.8	7.17	0.922		60.0
318	12.1	7.41	0.942		49.5
		Redlich–Peterson			
T (K)	A	B	g	R^2	SSE
303	9.80	0.288	0.977	0.927	40.8
313	17.7	0.703	0.882	0.922	58.4
318	17.8	0.574	0.924	0.942	42.4

Note: SSE = $\sum \left(q - q_c \right)^2$, q and q_c are the experimental value and calculated value according the model, respectively.

where K_L (L·mg^{-1}) is the Langmuir adsorption constant; R (J·mol^{-1}·K^{-1}) is the gas phase constant; T (K) is the temperature; $\Delta S°$ is the standard entropy change; $\Delta H°$ is the standard enthalpy change; $\Delta G°$ is the standard Gibbs free energy change; k is the adsorption rate constant obtained from the model which best fits the adsorption kinetic curve while A is pre-exponential factor.

The line thermodynamic analysis of the La-WS adsorption phosphate process is shown in Table 5. Since $\Delta G < 0$, $\Delta H > 0$, and $\Delta S > 0$, this indicated that the adsorption process of PO_4^{3-} onto La-WS was a spontaneous, endothermic and entropic adsorption process. The value of E_a was 24.0 kJ·mol^{-1} and this showed that the adsorption reaction was considered as physical adsorption when it ranged from 5 to 40 kJ·mol^{-1} [44]. In summary, the adsorption reaction was spontaneous and endothermic, and the adsorption process was accompanied by both chemical and physical reactions.

3.3. Column adsorption studies

The breakthrough curves at various conditions are presented in Fig. 6 and the results are calculated according to the breakthrough curves and listed in Table 6.

3.3.1. Comparison of phosphate adsorption on WS and La-WS and effect of salt

Fig. 6a shows the comparison of breakthrough curves about PO_4^{3-} adsorption on WS and La-WS. It was obviously observed from Fig. 6a that the breakthrough curve from WS is very steep and this indicated that the adsorption quantity of WS was enhanced after La modification. This again shows the modification is necessary to improve the adsorption quantity.

Fig. 6a also shows the effect of existed salt (NaCl) on breakthrough curve. It was clearly presented that there was slight effect about breakthrough about existed salt in influent. This shows that there is some tolerance about common salt about La-WS and this property is useful for adsorbent to remove pollutants from water.

3.3.2. Effect of column height

Effect of column height on breakthrough curves is shown in Fig. 6b. The higher the column height of La-WS, the longer it took to reach adsorption saturation. Since the higher the column was, the higher the amount of La-WS it contained, the more active sites could adsorb PO_4^{3-} and the less likely it was to reach equilibrium. It was clearly observed from Table 6 that values of Y became larger with the increase of column height while the values of q_e slightly increased.

3.3.3. Effect of influent concentration

Fig. 6c shows the effect of influent concentration. As the initial concentration of PO_4^{3-} increased, the time to reach equilibrium for dynamic adsorption of PO_4^{3-} on La-WS

Table 4
Fitting results of kinetic model toward PO_4^{3-} adsorption on La-WS

			Pseudo-first-order equation			
T (K)	C_0 (mg·L^{-1})	$q_{e(exp)}$ (mg·g^{-1})	$q_{e(theo)}$ (mg·g^{-1})	k_1 (min^{-1})	R^2	SSE
	10	16.2	16.0	0.122	0.963	2.51
303	20	26.8	26.1	0.093	0.974	6.68
	40	31.9	30.8	0.152	0.827	30.3
	10	17.7	16.9	0.0952	0.884	11.2
313	20	27.4	26.3	0.0956	0.951	12.0
	40	33.5	31.6	0.165	0.629	69.3
	10	17.9	17.7	0.148	0.969	2.05
318	20	27.9	27.1	0.113	0.965	7.65
	40	34.9	32.6	0.181	0.607	72.9
			Pseudo-second-order equation			
T (K)	C_0 (mg·L^{-1})	$q_{e(exp)}$ (mg·g^{-1})	$q_{e(theo)}$ (mg·g^{-1})	k_2 (g·mg^{-1}·min^{-1})	R^2	SSE
	10	16.2	16.9	0.0124	0.963	2.49
303	20	26.8	27.8	0.0054	0.969	7.90
	40	31.9	32.4	0.0082	0.973	4.81
	10	17.7	18.1	0.0083	0.986	1.31
313	20	27.4	28.2	0.0054	0.991	2.16
	40	33.5	33.5	0.0078	0.911	16.7
	10	17.9	18.6	0.0141	0.943	3.79
318	20	27.9	28.8	0.0065	0.978	4.70
	40	34.9	34.5	0.00823	0.895	19.6
			Elovich equation			
T (K)	C_0 (mg·L^{-1})	$q_{e(exp)}$ (mg·g^{-1})	α	β	R^2	SSE
	10	16.2	186	0.591	0.718	18.9
303	20	26.8	58.9	0.294	0.772	57.7
	40	31.9	1066	0.343	0.827	30.3
	10	17.7	35.7	0.447	0.896	9.98
313	20	27.4	60.8	0.299	0.835	40.6
	40	33.5	631	0.312	0.954	8.60
	10	17.9	817	0.619	0.657	22.7
318	20	27.9	161	0.321	0.760	52.0
	40	34.9	972	0.315	0.940	11.1

Table 5
Thermodynamic parameters for the adsorption of La-WS on PO_4^{3-}

E_a (kJ·mol^{-1})	ΔH (kJ·mol^{-1})	ΔS (J·mol^{-1}·K^{-1})	ΔG (kJ·mol^{-1})		
			303 K	313 K	318 K
24.0	25.7	91.2	–1.95	–2.78	–3.33

became shorter. Under the conditions of column height and flow rate, the total adsorption amount of La-WS increased with the increase of PO_4^{3-} concentration, but the removal efficiency of PO_4^{3-} decreased. With the increase of PO_4^{3-} concentration, the unit adsorption amount of La-WS on PO_4^{3-} also increased (Table 6). This was consistent with the results obtained in batch adsorption experiments.

3.3.4. Effect of flow rate

The effect of flow rate on breakthrough curve is presented in Fig. 6d. It can be seen from Fig. 6d that when the flow rate increased, the slope of the curve increased, the adsorption of La-WS on PO_4^{3-} decreased, and the removal effect became worse. Since the contact time between La-WS and PO_4^{3-} decreased when the flow rate was too high, the opportunity to bind the active site decreased, resulting in lower adsorption, so the adsorption process was more suitable for low flow rate. But seen in Table 6, the values of q_e slightly increased with the increase of flow rate.

As shown in Fig. 6, under the conditions of constant flow rate, column height and initial concentration, the unit adsorption amount increased rapidly with the increase of time, and then the increase became slow until the equilibrium was reached. When the adsorption time was certain, the
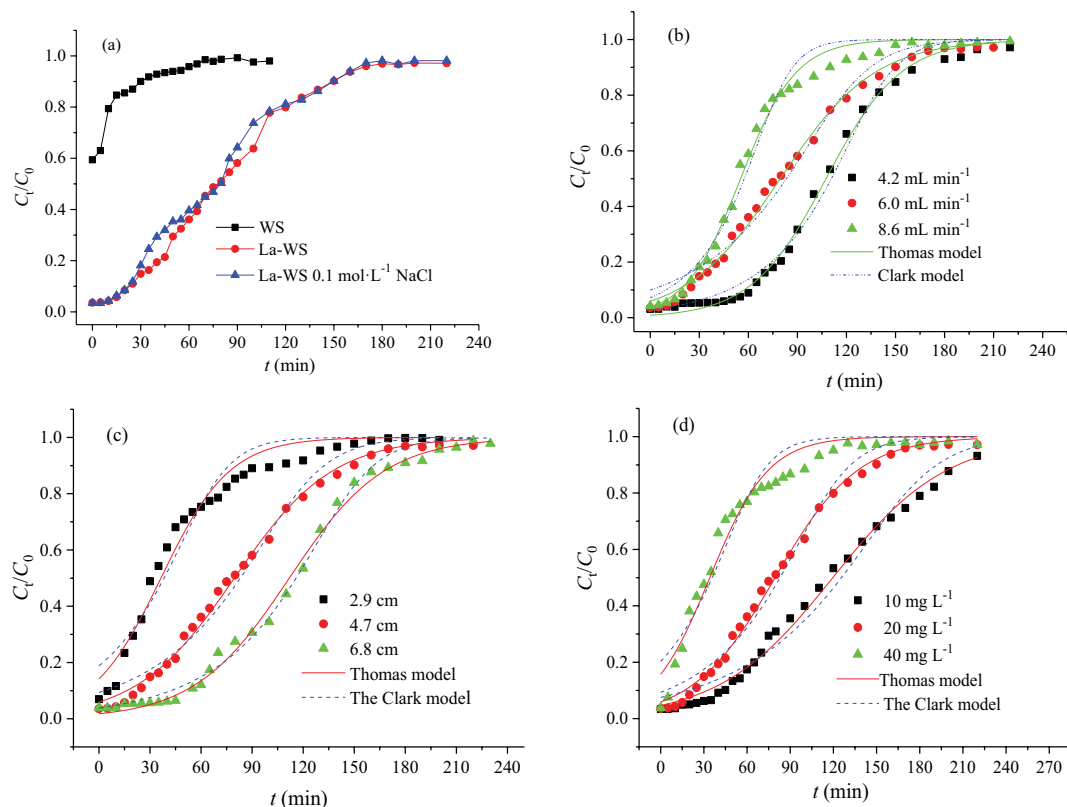
Fig. 6. Breakthrough curves of PO_4^{3-} adsorption: (a) comparison and effect of salt; effect of (b) flow rate, (c) column height, and (d) influent concentration.

Table 6
Results calculated from breakthrough curves at various conditions

No.	Z (cm)	v (mL·min^{-1})	C_0 (mg·L^{-1})	Q_m (mg)	W_{total} (mg)	Y (%)	q_e (mg·g^{-1})	t (min)
1	2.9	6	20	5.23	24.0	21.8	16.5	200
2	4.7	6	20	9.96	26.4	37.7	17.1	220
3	6.8	6	20	13.4	27.6	43.4	17.3	230
4	4.7	6	10	7.17	13.2	54.3	12.4	220
5	4.7	6	40	10.2	52.8	19.3	17.7	220
6	4.7	4.2	20	9.49	19.3	49.2	16.5	230
7	4.7	8.6	20	10.3	37.8	27.2	17.9	220

lower the flow rate, the higher the column height and initial concentration, and the higher the unit adsorption capacity.

3.3.5. Model fitting of dynamic adsorption curves

In order to find the equilibrium adsorption amount of PO_4^{3-} adsorbed by La-WS under different conditions and the characteristic parameters of adsorption, the experimental data of PO_4^{3-} adsorbed by La-WS at different flow rates, different initial concentrations and different column heights were fitted using Thomas model and The Clark model (expression of model shown in Table 2), and the results are shown in Fig. 6b–d and Table 7, respectively.

As could be seen from Table 7, the unit adsorption amount fitted by the Thomas model was close to the experimental

value, and the R^2 was larger and the SSE value was smaller. Moreover, the fitted curves from Thomas model were closer to experimental points. These inferred that Thomas model can better describe the process of PO_4^{3-} adsorption in column mode. Compared with Thomas model, the values of R^2 obtained from the Clark model were smaller while the values of SSE were larger, indicating that the Clark model was not well suitable to describe the process of PO_4^{3-} adsorption on La-WS.

3.4. Desorption regeneration studies

The adsorption–desorption experiments were conducted to investigate the regeneration ability of the adsorbent, so as to achieve the reuse of the material and reduce the cost [45–47].

Table 7
Results of column model non-linear fitting of La-WS toward PO_4^{3-}

			Thomas				
Z (cm)	v (mL·min^{-1})	C_0 (mg·L^{-1})	K_{Th} (mL·mg^{-1}·min^{-1})	$q_{0(theo)}$ (mg·g^{-1})	$q_{e(exp)}$ (mg·g^{-1})	R^2	SSE
2.9	6	20	2.50	13.7	16.5	0.973	0.0678
4.7	6	20	1.74	15.7	17.3	0.996	0.0150
6.8	6	20	1.79	17.2	18.7	0.996	0.0175
4.7	6	10	2.53	12.5	12.4	0.993	0.0842
4.7	6	40	1.23	14.3	17.7	0.965	0.0842
4.7	4.2	20	2.19	15.7	16.5	0.997	0.0124
4.7	8.6	20	2.95	16.5	17.9	0.992	0.0309
			Clark				
Z (cm)	v (mL·min^{-1})	C_0 (mg·L^{-1})	n	r_c	A	R^2	SSE
2.9	6	20	3.76	0.0755	103	0.949	0.129
4.7	6	20	3.76	0.0587	733	0.983	0.0572
6.8	6	20	3.76	0.0628	8390	0.994	0.0239
4.7	6	10	3.76	0.0429	1264	0.974	0.0666
4.7	6	40	3.76	0.0736	80.9	0.938	0.149
4.7	4.2	20	3.76	0.0729	18611	0.996	0.662
4.7	8.6	20	3.76	0.0960	1448	0.997	0.410
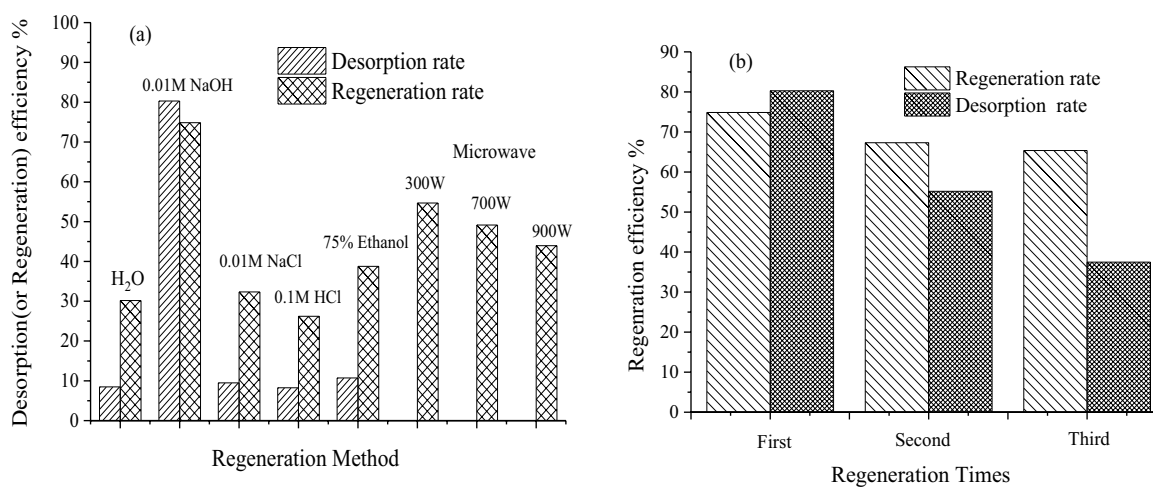
Fig. 7. Desorption and regeneration effects of multiple methods (a) and three regeneration effects of 0.01 mol·L^{-1} NaOH (b).

3.4.1. Desorption studies in batch mode

The results of desorption experiments and regeneration are shown in Fig. 7a and b. In the first desorption regeneration case, the best results were obtained when La-WS was desorbed and regenerated using 0.1 mol·L^{-1} NaOH solution, with a desorption efficiency of 80.3% and a regeneration efficiency of 74.9% while there was lower desorption or regeneration efficiency about other methods. From the effects of pH and salinity on the adsorption process, it was clear that the adsorption mainly relies on the ligand exchange interaction between La-WS and phosphate to form complexes. Due to the addition of strong bases, they formed competitive adsorption with phosphate, destroying their structure and releasing PO_4^{3-} to achieve desorption. The better effect

0.01 mol·L^{-1} NaOH solution was selected for three times of desorption regeneration, and the results are shown in Fig. 7b. The regeneration efficiencies of the first three times were 74.9%, 67.3% and 65.4%. The changes of the desorption efficiencies were the same as the regeneration efficiencies, which were 80.3%, 55.2% and 47.5% in the first three times. The above results indicated that La-WS was relatively stable as an adsorbent and could be reused several times.

3.4.2. Desorption studies in column mode

A certain amount of La-WS was weighed and loaded onto the column for adsorption of phosphate solution, and after the adsorption was completed, 0.01 mol·L^{-1} NaOH

Fig. 8. Effect of dynamic desorption and regeneration of PO_4^{3-} by La-WS (a) desorption and (b) regeneration.

Fig. 9. Schematic diagram of the mechanism of La-WS adsorption on PO_4^{3-}.

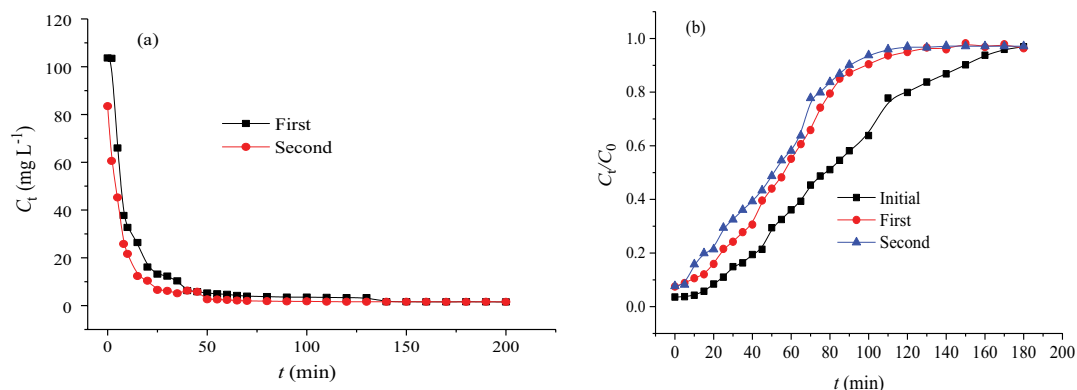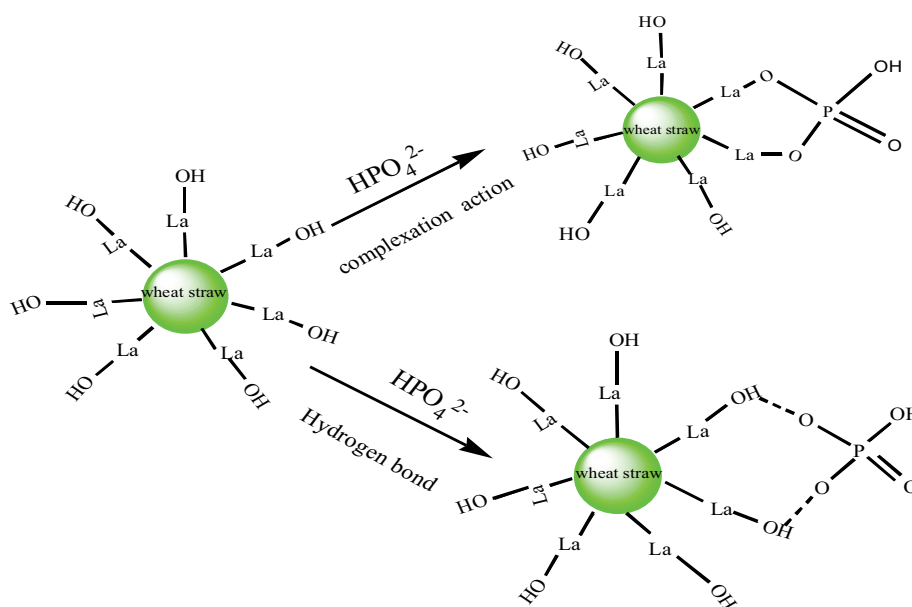solution was used for the desorption. The desorption results are shown in Fig. 8a and the regeneration results are shown in Fig. 8b. The desorption of spent La-WS using NaOH was fast when it is performed in Fig. 8a, and then it decreased rapidly and gradually tended to equilibrium. The curves of the three adsorptions follow the same trend as seen in Fig. 8b, and the curves of the first adsorption and the first regeneration basically matched, which also indicated that the adsorption effect of La-WS was better after regeneration. The unit adsorption amount was 17.0 mg·g⁻¹ for the first adsorption, 11.8 mg·g⁻¹ for the first regeneration, and 10.6 mg·g⁻¹ for the second regeneration, and the desorption rates were 98.8% and 90.5% for the two adsorptions. The regeneration rates were 69.7% and 62.7% for the adsorption process. Compared with the batch desorption and regeneration, the regeneration efficiencies was not much different, but the desorption efficiencies was higher, indicating that the 0.01 mol·L⁻¹ NaOH solution was more effective for the desorption of PO_4^{3-}-loaded La-WS, and the multiple regeneration of La-WS was not effective.

3.5. Adsorption mechanism

The experiments showed that La-WS had good selective adsorption effect on PO_4^{3-}. Based on the effects of pH and coexisting ions on the adsorption of PO_4^{3-} by La-WS, it was shown that anion exchange or electrostatic gravitation was not the main adsorption mechanism, and the main adsorption mechanism of La-WS on PO_4^{3-} was ligand exchange. pH was around 7, and the phosphate was mainly in the form of $H_2PO_4^-$ and HPO_4^{2-} [48]. In this paper, the adsorption of La-WS on PO_4^{3-} also showed good adsorption at pH 7. The kinetic and thermodynamic analysis showed that the adsorption of PO_4^{3-} by La-WS was mainly chemisorption (coordination reaction) accompanied by physical adsorption (electrostatic reaction) [42], the isotherm fitting results indicated that the adsorption process was dominated by monomolecular layer chemisorption. in addition, La-WS would form hydrogen bonding interaction with PO_4^{3-}. The adsorption mechanism of La-WS on PO_4^{3-} was shown in Fig. 9.

4. Conclusion

La-WS showed good adsorption property toward phosphate. When the pH was between 3 and 7, the adsorption process of La-WS on PO_4^{3-} was favored. And the presence of salinity had little effect on the adsorption. The Langmuir and Redlich–Peterson models could be used to describe the equilibrium adsorption while the pseudo-second-order model could better describe the kinetic process of PO_4^{3-} adsorption onto La-WS. The adsorption process was spontaneous and endothermic, accompanied by both chemical and physical reactions. The column adsorption studies showed that the lower the flow rate, the higher the column height and initial concentration were advantage of adsorption capacity. The process of PO_4^{3-} adsorption by La-WS was well described by the Thomas model. The relative stability of the adsorbent La-WS and its ability to be reused many times were demonstrated, with the best results when La-WS was desorbed and regenerated using 0.1 mol·L^{-1} NaOH solution. The obtained La-WS not only has selective adsorption on phosphate, but also has a good application prospect because of its relative stability and reuse.

Acknowledgements

References

[1] N.Y. Acelas, B.D. Martin, D. Lopez, B. Jefferson, Selective removal of phosphate from wastewater using hydrated metal oxides dispersed within anionic exchange media, Chemosphere, 119 (2015) 1353–1360.

[2] M.N. Kumwimba, M. Dzakpasu, X.Y. Li, Potential of invasive watermilfoil (*Myriophyllum* spp.) to remediate eutrophic water-bodies with organic and inorganic pollutants, J. Environ. Manage., 270 (2020) 110919, doi: 10.1016/j.jenvman.2020.110919.

[3] B.K. Mayer, L.A. Baker, T.H. Boyer, P. Drechsel, M. Gifford, M.A. Hanjra, P. Parameswaran, J. Stoltzfus, P. Westerhoff, B.E. Rittmann., Total value of phosphorus recovery, Environ. Sci. Technol., 50 (2016) 6606–6620.

[4] C.X. Li, Y. Yu, Q.Y. Li, H. Zhong, S. Wang, Kinetics and equilibrium studies of phosphate removal from aqueous solution by calcium silicate hydrate synthesized from electrolytic manganese residue, Adsorpt. Sci. Technol., 37 (2019) 547–565.

[5] M.Y. Zhang, Y.Z. Chi, S.Y. Li, C.L. Fu, H.Y. Yuan, X.K. Wang, F.Q. Chen, Chemical phosphorus removal optimization from coating wastewater using iron-calcium salt, Desal. Water Treat., 264 (2022) 164–171.

[6] Q. Guan, G.S. Zeng, B.C.A. Gong, Y.P. Li, H.Y. Ji, J.F. Zhang, J.T. Song, C.L. Liu, Z.B. Wang, C.J. Deng, Phosphorus recovery and iron, copper precipitation from swine wastewater via struvite crystallization using various magnesium compounds, J. Cleaner Prod., 328 (2021) 129588, doi: 10.1016/j.jclepro.2021.129588.

[7] Z.Q. Zhu, C.P. Huang, Y.N. Zhu, W.H. Wei, H. Qin, A hierarchical porous adsorbent of nano-alpha-Fe_2O_3/Fe_3O_4 on bamboo biochar (HPA-Fe/C-B) for the removal of phosphate from water, J. Water Process Eng., 25 (2018) 96–104.

[8] H. Zhang, S.S. Zhang, L. Zhu, Y.P. Li, L. Chen, Phosphorus recovery in the alternating aerobic/anaerobic biofilm system: performance and mechanism, Sci. Total Environ., 810 (2022) 152297, doi: 10.1016/j.scitotenv.2021.152297.

[9] Y.J. Dai, W.S. Wang, L. Lu, L.L. Yan, D.Y. Yu, Utilization of biochar for the removal of nitrogen and phosphorus, J. Cleaner Prod., 257 (2020) 120573, doi: 10.1016/j.jclepro.2020.120573.

[10] K.Y.A. Lin, S.Y. Chen, A.P. Jochems, Zirconium-based metal organic frameworks: highly selective adsorbents for removal of phosphate from water and urine, Mater. Chem. Phys., 160 (2015) 168–176.

[11] A.K.A. Khalil, F. Dweiri, I.W. Almanassra, A. Chatla, M.A. Atieh, Mg-Al layered double hydroxide doped activated carbon composites for phosphate removal from synthetic water: adsorption and thermodynamics studies, Sustainability, 14 (2022) 6911, doi: 10.3390/su14126991.

[12] W.Y. Huang, J. Chen, F. He, J.P. Tang, D. Li, Y. Zhu, Y.M. Zhang, Effective phosphate adsorption by Zr/Al-pillared montmorillonite: insight into equilibrium, kinetics and thermodynamics, Appl. Clay Sci., 104 (2015) 252–260.

[13] G.J. Jiao, J.L. Ma, Y.C. Li, D. Jin, Z. Ali, J.H. Zhou, R.C. Sun, Recent advances and challenges on removal and recycling of phosphate from wastewater using biomass-derived adsorbents, Chemosphere, 278 (2021) 130377, doi: 10.1016/j.chemosphere.2021.130377.

[14] S.Q. Tian, R.Y. Zhao, Z.C. Chen. Review of the pretreatment and bioconversion of lignocellulosic biomass from wheat straw materials, Renewable Sustainable Energy Rev., 91 (2018) 483–489.

[15] S. Mashhadi, H. Javadian, M. Ghasemi, T.A. Saleh, V.K. Gupta, Microwave-induced H_2SO_4 activation of activated carbon derived from rice agricultural wastes for sorption of methylene blue from aqueous solution, Desal. Water Treat., 57 (2016) 21091–21104.

[16] X.X. Shi, Y.Y. Qiao, X.X. An, Y.Y. Tian, H.F. Zhou, High-capacity adsorption of Cr(VI) by lignin-based composite: characterization, performance and mechanism, Int. J. Biol. Macromol., 159 (2020) 839–849.

[17] H.L. Zhang, M. Elskens, G.X. Chen, L. Chou, Phosphate adsorption on hydrous ferric oxide (HFO) at different salinities and pHs, Chemosphere, 225 (2019) 352–359.

[18] X.J. Xing, W. Jiang, S. Li, X.W. Zhang, W.Q. Wang, Preparation and analysis of straw activated carbon synergetic catalyzed by $ZnCl_2$-H_3PO_4 through hydrothermal carbonization combined with ultrasonic assisted immersion pyrolysis, Waste Manage., 89 (2019) 64–72.

[19] N.S. Trivedi, R.A. Kharkar, S.A. Mandavgane, Use of wheat straw combustion residues for removal of chlorinated herbicide (2,4-dichlorophenoxyacetic acid), Waste Biomass Valorization, 10 (2019) 1323–1331.

[20] D. Jin, W.F. Dong, H.T. Zhang, Y.H. Ci, L.P. Hou, L.H. Zang, F.G. Kong, L. Lucia, Comparison of structural characteristics of straw lignins by alkaline and enzymatic hydrolysis, BioResources, 14 (2019) 5615–5629.

[21] Y.Y. Su, B.L. Zhao, W. Xiao, R.P. Han Adsorption behavior of light green anionic dye using cationic surfactant-modified wheat straw in batch and column mode, Environ. Sci. Pollut. Res., 20 (2013) 5558–5568.

[22] L.Y. Han, X. Liu, P.F. Yang, R.P. Han, Adsorption of phosphate by Cu-loaded polyethylenimine modified wheat straw, Desal. Water Treat., 274 (2022) 230–238.

[23] S.H. Mood, M. Ayiania, H.L. Cao, O. Marin-Flores, Y.J. Milan, M. Garcia-Perez, Nitrogen and magnesium Co-doped biochar for phosphate adsorption, Biomass Convers. Biorefin., (2021), doi: 10.1007/s13399-021-01404-1.

[24] M.X. Tang, R. Zhang, Y.W. Pu, Wheat straw modified with palmitic acid as an efficient oil spill adsorbent, Fibers Polym., 19 (2018) 949–955.

[25] Z.H. Ma, Q. Li, Q.Y. Yue, B.Y. Gao, W.H. Li, X. Xu, Q.Q. Zhong, Adsorption removal of ammonium and phosphate from water by fertilizer controlled release agent prepared from wheat straw, Chem. Eng. J., 171 (2011) 1209–1217.

[26] M.Y. Han, J.H. Zhang, Y.Y. Hu, R.P. Han, Preparation of novel magnetic microspheres with La and Ce-bimetal oxide shell for excellent adsorption of fluoride and phosphate from solution, J. Chem. Eng. Data, 64 (2019) 3641–3651.

[27] W.T. Fan, F. Zhao, J.H. Dou, X.H. Guo, Continuous preparation of dual-mode luminescent LaPO$_4$:Tb^{3+},Yb^{3+} nanoparticles by reactive flash nanoprecipitation, Chem. Eng. Sci., 239 (2021) 116734, doi: 10.1016/j.ces.2021.116734.

[28] H.J. Duan, L. Zhang, Y.L. Wang, Y.H. Liu, Y.Y. Wang, Phosphate removal from aqueous solution by Fe-La binary (hydr)oxides: characterizations and mechanisms, Environ. Sci. Pollut. Res., 28 (2021) 62662–62676.

[29] Y.L. Wang, Y.H. Liu, T.Q. Guo, H.P. Liu, J.L. Li, S.F. Wang, X.H. Li, X. Wang, Y.F. Jia, Lanthanum hydroxide: a highly efficient and selective adsorbent for arsenate removal from aqueous solution, Environ. Sci. Pollut. Res., 27 (2020) 42868–42880.

[30] X. Zhang, S. Zhang, X. Wang, Y. Wang, S. Li, G. Wang, Removal of phosphorus from wastewater by lanthanum-modified straws, Environ. Chem., 40 (2021) 1274–1284.

[31] Y.M. Huang, X.Q. Lee, M. Grattieri, M.W. Yuan, R. Cai, F.C. Macazo, S.D. Minteer, Modified biochar for phosphate adsorption in environmentally relevant conditions, Chem. Eng. J., 380 (2020) 122375, doi: 10.1016/j.cej.2019.122375.

[32] M.Y. Liu, X.T. Zhang, Z.H. Li, L.B. Qu, R.P. Han, Fabrication of zirconium(IV)-loaded chitosan/Fe$_3$O$_4$/graphene oxide for efficient removal of alizarin red from aqueous solution, Carbohydr. Polym., 248 (2020) 116792, doi: 10.1016/j.carbpol.2020.116792.

[33] X.T. Zhang, C.H. Ma, K. Wen, R.P. Han, Adsorption of phosphate from solution by lanthanum-modified macroporous chelating resin, Korean J. Chem. Eng., 37 (2020) 776–775.

[34] J.L. Wang, X. Liu, M.M. Yang, H.Y. Han, S.S. Zhang, G.F. Ouyang, R.P. Han, Removal of tetracycline using modified wheat straw from solution in batch and column modes, J. Mol. Liq., 338 (2021) 116698, doi: 10.1016/j.molliq.2021.116698.

[35] R. Xu, M.Y. Zhang, R.J.G. Mortimer, G. Pan, Enhanced phosphorus locking by novel lanthanum/aluminum-hydroxide composite: Implications for eutrophication control, Environ. Sci. Technol., 51 (2017) 3418–3425.

[36] M. Bortolotti, L. Lutterotti, G. Pepponi. Combining XRD and XRF analysis in one Rietveld-like fitting, Powder Diffr., 32 (2017) S225–S230.

[37] X.D. Li, Y. Kuang, J.B. Chen, D.Y. Wu, Competitive adsorption of phosphate and dissolved organic carbon on lanthanum-modified zeolite, J. Colloid Interface Sci., 574 (2020) 197–206.

[38] L.P. Fang, Q.T. Shi, J. Nguyen, B.L. Wu, Z.M. Wang, I.M.C. Lo, Removal mechanisms of phosphate by lanthanum hydroxide nanorods: Investigations using EXAFS, ATR-FTIR, DFT, and surface complexation modeling approaches, Environ. Sci. Technol., 51 (2017) 12377–12384.

[39] L. Zhang, Y.H. Liu, Y.L. Wang, X.H. Li, Y.Y. Wang, Investigation of phosphate removal mechanisms by a lanthanum hydroxide adsorbent using p-XRD, FTIR and XPS, Appl. Surf. Sci., 557 (2021) 149838, doi: 10.1016/j.apsusc.2021.149838.

[40] W. Zhang, J. Fu, G.S. Zhang, X.W. Zhang, Enhanced arsenate removal by novel Fe-La composite (hydr)oxides synthesized via coprecipitation, Chem. Eng. J., 251 (2014) 69–79.

[41] R.T. Liu, L.N. Chi, X.Z. Wang, Y. Wang, Y.M. Sui, T.T. Xie, H. Arandiyan, Effective and selective adsorption of phosphate from aqueous solution via trivalent-metals-based amino-MIL-101 MOFs, Chem. Eng. J., 357 (2019) 159–168.

[42] Y.F. Gu, M.M. Yang, W.L. Wang, R.P. Han, Phosphate adsorption from solution by zirconium-loaded carbon nanotubes in batch mode, J. Chem. Eng. Data, 64 (2019) 2849–2858.

[43] Y. Wang, X.M. Xie, X.L. Chen, C.H. Huang, S. Yang, Biochar-loaded Ce^{3+}-enriched ultra-fine ceria nanoparticles for phosphate adsorption, J. Hazard. Mater., 396 (2020) 122626, doi: 10.1016/j.jhazmat.2020.122626.

[44] S. Chen, C.X. Qin, T. Wang, F.Y. Chen, X.L. Li, H.B. Hou, M. Zhou, Study on the adsorption of dyestuffs with different properties by sludge-rice husk biochar: adsorption capacity, isotherm, kinetic, thermodynamics and mechanism, J. Mol. Liq., 285 (2019) 62–74.

[45] A.A. Aryee, F.M. Mpatani, Y.Y. Du, A.N. Kani, E. Dovi, R.P. Han, Z.H. Li, L.B. Qu, Fe$_3$O$_4$ and iminodiacetic acid modified peanut husk as a novel adsorbent for the uptake of Cu(II) and Pb(II) in aqueous solution: characterization, equilibrium and kinetic study, Environ. Pollut., 268 (2021) 115729, doi: 10.1016/j.envpol.2020.115729.

[46] H.N. Bhatti, Z. Mahmood, A. Kausar, S.M. Yakout, O.H. Shair, M. Iqbal, Biocomposites of polypyrrole, polyaniline and sodium alginate with cellulosic biomass: adsorption–desorption, kinetics and thermodynamic studies for the removal of 2,4-dichlorophenol, Int. J. Biol. Macromol., 153 (2020) 146–157.

[47] H.J. Wang, Q. Liu, Z.Q. Wang, R.P. Han, Adsorption of CDMA from solution in batch mode using chemical activated pyrolytic char, Desal. Water Treat., 231 (2021) 367–376.

[48] R. Xue, R. Xu, L. Gu, L.H. Pan, Q. He, Study of phosphorus removal by using sponge iron adsorption, Water Air Soil Pollut., 229 (2018) 161, doi: 10.1007/s11270-018-3753-x.